Am J Transl Res 2022;14(3):1991-2001
www.ajtr.org /ISSN:1943-8141/AJTR0139510

Original Article

ICG-ER: a new probe for photoimaging and photothermal therapy for breast cancer

Yu Weng[1*], Zheng-Jie Wang[1*], Teng-Yu Guo[3], Wen-Bo Li[1], Yi-Yi Cao[1], Rui Zuo[1], Peng-Fei Xu[2], Hua Pang[1]

[1]Department of Nuclear Medicine, The First Affiliated Hospital of Chongqing Medical University, Chongqing 400016, P. R. China; [2]Institute of Clinical Pharmacy & Pharmacology, Jining First People's Hospital, Jining Medical University, Jining 272000, P. R. China; [3]College of Chemistry, Jilin University, Changchun 130012, P. R. China. [*]Equal contributors.

Received September 29, 2021; Accepted March 3, 2022; Epub March 15, 2022; Published March 30, 2022

Abstract: Breast cancer is common cancer type with high mortality. There are still inperfections in the traditional diagnosis and treatment methods for cancer. Photoacoustic imaging combines the advantages of high specificity and deep tissue penetration and is especially suitable for early cancer detection and treatment monitoring. With its specificity and noninvasiveness; photothermal therapy has become one of the best representative treatment methods. Indocyanine green (ICG) is a near-infrared imaging reagent approved by the FDA for clinical application, with a potential application for photothermal therapy. ICG has low targeting specificity. Through the combination of EB and ICG, the timeliness of ICG circulation *in vivo* is improved, and the tumor targeting of ICG-E is improved by using RGD. ICG-ER, an integrated optical probe for diagnosis and treatment, was constructed, and high uptake of ICG-ER by 4T1 cells was observed by flow cytometry and confocal laser scanning microscopy (CLSM). ICG-ER photoacoustic signal intensity is concentration-dependent. *In vivo* photoacoustic imaging showed that the ICG-ER concentration time in the tumor site was long and reached a peak at 42 hours. Under laser irradiation, the temperature of the tumor site in mice that were injected with ICG-ER reached 56°C. After photothermal treatment, the tumor tissue in the mice showed obvious necrosis and no tumor recurrence, proving that ICG-ER has a good photothermal effect. Based on the above results, ICG-ER can be used in breast cancer optical imaging and photothermal therapy, which is expected to provide new ideas for breast cancer clinical diagnosis and treatment.

Keywords: Breast cancer, indocyanine green, Evans blue, photoacoustic imaging, photothermal therapy

Introduction

With the development and progress of science and technology, human exploration of cancer diagnosis and treatment has also made advancements. However, as an aggressive type of cancer, breast cancer has a high mortality rate. Currently, breast cancer imaging diagnosis methods include X-ray, ultrasound, and MRI, but X-rays have radioactivity, ultrasound has a strong subjectivity, and MRI has a low specificity in breast cancer diagnosis [1-3]. Photoacoustic imaging (PAI) combines the advantages of high specificity in pure optical tissue imaging and deep penetration in pure ultrasonic tissue imaging. It can obtain tissue images with high resolution and high contrast, avoiding the influence of light scattering, in principle [4]. Traditional breast cancer treatment includes surgery, chemotherapy, and radiotherapy. Although it has specific curative effects, there are problems of trauma, specificity, and systemic toxicity which have always been confusing [5-7]. Photothermal therapy (PTT) improves the management of the above issues and has become one of the most representative treatment methods [8-11].

Currently, photothermal conversion agents are mainly inorganic materials and organic dyes [12]. At present, there have been many PTCAs used in research. Indocyanine green (ICG), as the only organic dye approved by clinical practice, has been widely used in liver surgery [13]. Some studies have shown ICG being used in breast cancer's sentinel lymph node (SLN) location [14-16], which makes it possible to apply ICG in photoacoustic imaging and photothermal

treatment of breast cancer. However, ICG lacks tumor targeting and has a short half-life in the blood, which undoubtedly increases the difficulty of ICG in diagnosing breast cancer tumors [17-19].

EB has a long history of being used as a biofuel and clinical diagnostic reagent [20]. Bobin and other researchers evaluated the feasibility of sentinel lymph node identification in 100 patients with breast cancer, which proved the dye's sensitivity in detecting lymph node metastasis [21]. Integrin $\alpha_V\beta_3$ receptor is an essential target for tumor angiogenesis drug design. Arg-Gly-Asp (RGD) can be recognized by the integrin $\alpha_V\beta_3$ receptor [22, 23]. Therefore, research on RGD-containing peptides as tumor angiogenesis imaging agents and therapeutic drugs is also a current research focus [24-27]. We successfully combined EB with ICG to form ICG-E. Then, we combined ICG-E with c(RGDfc) to obtain ICG-ER (**Figure 7**), and assume that this will make ICG-E more effective in tumor targeting.

This study combined ICG with EB and RGD to obtain ICG-ER. ICG is used for optical imaging and photothermal therapy, EB is used to increase ICG uptake and residence time in tumors, and RGD is used to target $\alpha_V\beta_3$ integrin overexpressed on tumor angiogenesis endothelial cells. ICG-ER has good optical imaging ability and stability.

Material and methods

Materials and reagents

All chemical reagents were obtained from the commercial suppliers and used without further purification. MALDITOF-MS spectra were obtained by an AB SCIEX 4700 TOF/TOF System. UV-vis was tested with a Shimadzu Model UV-1700 spectrometer. FSL1000 fluorescence spectrophotometer (FSL1000, Edinburgh Instruments Ltd.) equipped with the Quantum Yield measuring accessory and Report Generator program was used for photoluminescence (PL) spectra study and Absolute Quantum Yield Measurement. Flash chromatography was performed on 200-400 mesh silica. Thin layer chromatography was performed using silica gel 60G F254 25 glass plates and visualized under 254/365 nm ultraviolet light. NIR-II *in vivo* imaging was performed on a small animal imaging system with fiber-coupled 915 nm laser system. Propidium iodide (PI) and a cell counting kit (CCK-8) were made in Dojindo (Japan). The plasma water was from a Millipore water purification system. Other reagents were used without further purification.

Synthesis of ICG-ER

Synthesis of ICG-E: EB-Mal was prepared according to previous work [28]. ICG-NHS (16 mg, 1 eq) in 3 mL anhydrous N, N-dimethylformamide (DMF) was stirred with EB-Mal (16 mg, 1.1 eq) with the addition of DIPEA (3 eq). Then, the mixture was stirred under an N^2 atmosphere at room temperature. The reaction was monitored by HPLC analysis and completed in 4 hours. The mobile phases (A) demineralized water and (B) acetonitrile were acidified to pH 3 with trifluoroacetic acid. Gradient elution was performed as follows: 10% B, 0-3 min; 10-90% B, 3-12 min; 90% B, 12-16 min; 90-10% B, 16-18 min; and 10% B, 18-20 min. The product was purified by Pro-HPLC (Figure S4). MALDI-TOF-MS analysis confirmed a mass of 1534.58 $[M]^+$ with an isolated yield of 53% (7.9 mg) (Figures S5, S6).

Synthesis of ICG-ER: ICG-E (1 eq, 15 mg) was dissolved in 0.5 mL of DMSO. RGD-SH (1.1 eq, 6.3 mg) was dissolved in 5 mL of degassed 0.1% sodium ascorbate (w/v) in phosphate-buffered saline (PBS), and added to the reaction solution. The reaction was stirred at RT for 2 h. The reaction mixture was monitored by analytical HPLC and purified by Pro-HPLC (Figure S7). The mobile phases (A) demineralized water and (B) acetonitrile were acidified to pH 3 with trifluoroacetic acid. Gradient elution was performed as follows: 10% B, 0-3 min; 10-90% B, 3-12 min; 90% B, 12-16 min; 90-10% B, 16-18 min; and 10% B, 18-20 min. MALDI-TOF-MS analysis confirmed a mass of 2110.583 $[M]^-$ with an isolated yield of 48% (10.2 mg) (Figure S8).

Cell culture and 4T1 tumor-bearing mice model

Murine breast cancer: 4T1 breast cancer cells were purchased from ATCC (Shanghai, China), and the full medium was prepared with RPMI-1640 medium (Gibco), 10% fetal bovine serum

(FBS), and 1% penicillin streptomycin antibody. The cells were incubated in an incubator of 5% CO_2 and 37°C. When the cells were cultured to 80% confluency, they were passed on at a ratio of 1:3 to carry out cell experiments and construct tumor models.

All animals (female BALB/c nude mice, weighing 18-22 g, aged 6-8 W) were purchased from the experimental animal center of Chongqing Medical University. All experiments and operations were carried out with the approval of guidelines from the Animal Care and Use Committee of the First Affiliated Hospital of Chongqing Medical University (Grant Nos. 82102093, ethical approval report has been provided to the Supplementary Data File). The cells were suspended in PBS (100 μl 1×10^6 4T1 cells per mouse) and then subcutaneously injected into the left hind limb of the female nude mice. The tumor volume was calculated by [$\pi/6 \times \text{length} \times (\text{width})^2$].

In vitro cytotoxicity and intracellular uptake of ICG-ER

4T1 cells in logarithmic growth phase were seeded in 96-well plates at a density of 2×10^4/ml well, and cultured in a cell incubator at 37°C and 5% CO_2 until more than 50% adherent. The experimental group (As) was cocultured with different concentrations of ICG-ER (10, 20, 30, 40, and 50 μg/ml) cell culture medium. Pure culture medium was set as the blank group (Ab), sterile culture medium plus cells as the control group (Ac), and 6 multiple wells were set at each concentration.

After 24 hours of culture, all cells were washed with PBS and then incubated with 100 μL of 10% CCK-8 reagent for 30 minutes in each well. The multifunctional microplate reader was set to scan at 450 nm. The cell survival rate was calculated according to the formula [(As-Ab)/(Ac-Ab)] ×100%.

To study the uptake of ICG and ICG-ER in tumor cells, 4T1 cells (5×10^4/ml) were placed in CLSM dishes. After 24 hours, the cells were cultured in a complete medium containing ICG or ICG-ER for 12 hours, and the nuclei were stained with PI. CLSM (Nikon A1, Japan) was used to record fluorescence images directly. In addition, the intracellular uptake of 4T1 cells, coincubated with ICG or ICG-ER for 12 h was measured by CytoFLEX flow cytometry (Beckman Coulter. Suzhou, China).

In vitro and in vivo PA imaging

To evaluate the PA imaging effect of ICG-ER, a gel model with a diameter of 5 mm was prepared. ICG-ER maximum absorbance in the range of 680 nm-970 nm (interval =5 nm) was measured by a VEVO LAZR photoacoustic imaging system (VisualSonics Inc., Toronto, Canada). Then, a laser at an excitation wavelength of 805 nm was used (Figure S9). Different concentrations (5, 10, 15, 20, and 25, μg/ml) of ICG-ER solution were used for PA imaging. Then, the region of interest (ROI) of each image was checked with VEVO LAZR software, and the PA intensity value of the region was measured. For *in vivo* PA imaging, nude mice bearing 4T1 tumors (n=3) were injected with ICG-ER (0.35 mg/ml) diluted with 10% Human serum albumin (HSA) via the tail vein. PA images were collected at different times (pre, 6 h, 12 h, 24, 36 h, 42 h), and the average PA intensity of the tumor area was measured.

In vitro photothermal effect

To better observe the influence of concentration on ICG-ER temperature under laser irradiation the following steps were performed. First, ICG-ER was diluted in different concentrations (10, 20, 40, 80, 160 μg/ml), and normal saline was used as a blank control. Second, diluted ICG-ER and normal saline were added to six 96-well plates. The 808 nm laser (1.5 W cm^{-2}) was used to irradiate for 400 s. Over time, the temperature changes of ICG-ER and normal saline at different concentrations were monitored with a thermal imager (Fourier 226, China).

In vivo photothermal therapy

To evaluate whether ICG-ER has the effect of photothermal therapy, mice with a tumor volume reaching 50-80 mm^3 were randomly divided into 4 groups (n=3). The first group was the control group, and 100 μl of normal saline was injected into the tail vein. In the second group, 100 μl 0.35 mg/ml ICG-ER solution was injected intravenously. In the third group, 100 μl of normal saline was injected into the tail vein and irradiated with an 808 nm laser (1.5 W cm^{-2}) for 10 minutes. The fourth group

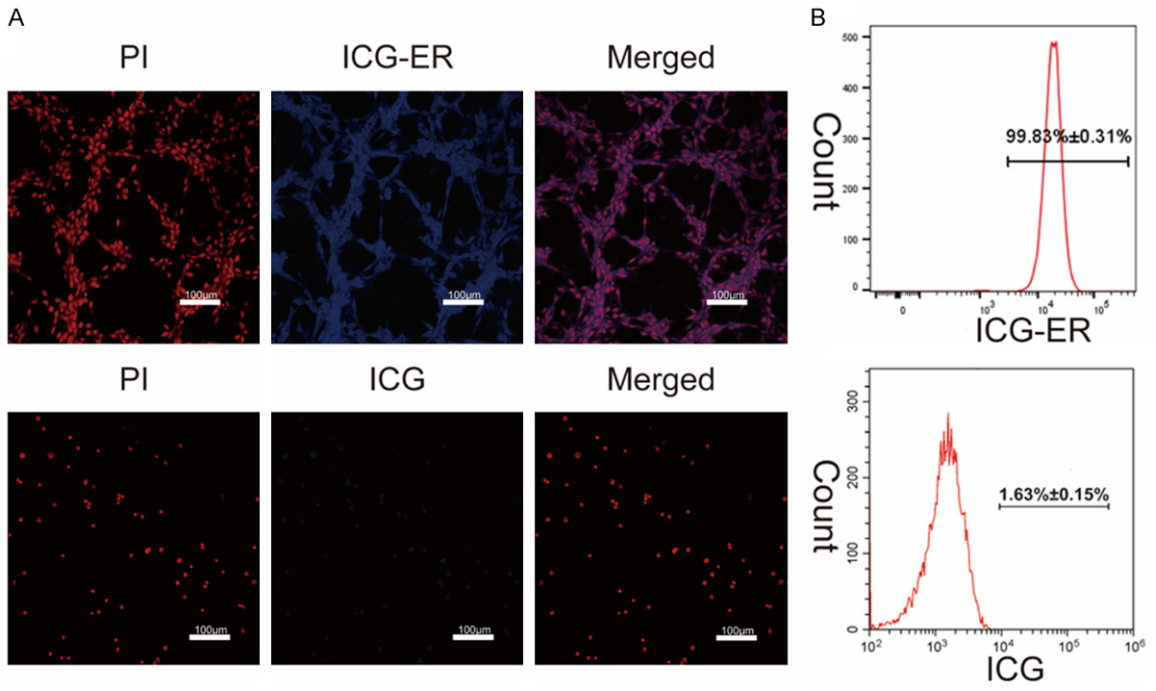

Figure 1. A. CLSM images of 4T1 cells coincubated with ICG-ER or ICG for 12 h. B. Flow cytometry analysis of intracellular uptake of ICG-ER and ICG. All images were observed under the CLSM at 200X magnification. The scale bars are 100 μm.

was the ICG-ER+laser group. One hundred microliters of 0.35 mg/ml ICG-ER was injected intravenously and irradiated with an 808 nm laser (1.5 W cm^{-2}) for 10 minutes. An infrared thermal imaging camera recorded the temperature change and infrared thermal images. The tumor volume and weight changes of the four groups of mice were recorded every two days after photothermal treatment. The tumor volume was calculated by V/V_0 (V_0: initial tumor volume before treatment). After 24 hours of photothermal treatment, blood, main organs (heart, liver, spleen, lung, kidney), and tumor tissue were harvested and fixed in 4% paraformaldehyde solution (n=3). To observe the biosafety of ICG-ER, ALT, AST, and BUN kits were used to detect renal function and liver function. The main organs were stained with H&E. Finally, H&E, PCNA, TUNEL, and HSP70 staining were performed analyze the histopathological changes in tumor tissue.

Statistical analysis

All statistical analyses were performed with SPSS 20.0 software. Data were presented as mean ± standard deviation. The significance of data was analyzed according to Student's t-test, one-way ANOVA and two-way ANOVA.

Results

Preparation and characterization of ICG-ER

ICG-E was easily synthesized through the direct conjugation of ICG-NHS with compound EB-Mal. The free thiol group of c(RGDfc) was covalently attached to the ICG-E maleimide motif to give the final ICG-ER product (**Figure 7**).

In vitro cytotoxicity and in vitro cell targeting

After the cells were incubated with ICG-ER for 24 h, the cell survival rate was calculated according to the CCK-8 method (Figure S1). The results showed that at the highest concentration (50 μg/ml), the cell survival rate reached more than 95%. This indicates that ICG-ER has very low biological toxicity.

To explore the targeting ability of ICG-ER and ICG on tumor cells, we observed the uptake of ICG-ER and ICG in 4T1 cells by CLSM. The results showed that ICG-ER was concentrated around the nucleus, whereas ICG did not pro-

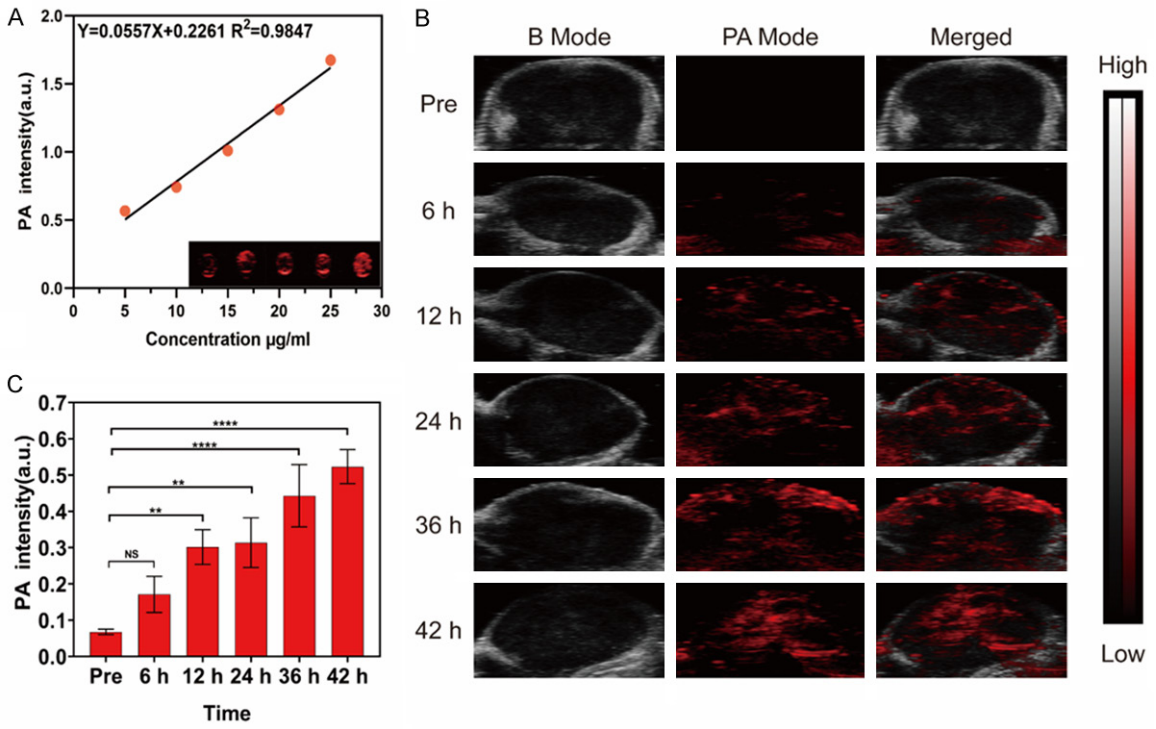

Figure 2. A. *In vitro* PA contrast images and PA values of different ICG-ER concentrations. B. *In vivo* PA images of tumors in 4T1 tumor-bearing mice after caudal vein injection of ICG-ER at different time points. C. Changes in PA signal intensities within tumor regions at corresponding time points. The intensity of the PA signal at different time points before and after ICG-ER injection was analyzed by one-way ANOVA, $^{**}P<0.01$, $^{****}P<0.0001$. (Values are means ± SD., n=3).

duce such an effect (**Figure 1A**). Flow cytometry results showed that the uptake of ICG-ER by 4T1 cells was 99.83%±0.31%, and the uptake of ICG was 1.63%±0.15% (**Figure 1B**). Both CLSM and flow cytometry showed that ICG-ER was more specific to tumor cells than ICG. These results provide evidence for ICG-ER photoacoustic imaging and photothermal therapy *in vivo*.

In vitro and in vivo PA imaging

PA is a new imaging method, and its sensitivity is better than that of CT [29]. Because ICG has strong absorbance in the near infrared region, ICG is often used as a PA contrast agent. We will use 10% HSA for ICG-ER diluted to different concentrations. At the concentrations of 5 μg/ml to 25 μg/ml, the PA signal was more pronounced. The PA signal intensity increased linearly with increasing ICG-ER concentration intensity (**Figure 2A**). PA images (**Figure 2B**) and signal values of the tumor site were recorded before and after ICG-ER was injected into the tail vein of nude mice. The PA signal in the tumor site was stronger with time and reached a peak value at 42 h (**Figure 2C**). This indicates that ICG-ER can be a PA contrast agent *in vivo*.

In vitro photothermal effect

To evaluate the photothermal properties of ICG-ER, different concentrations of ICG-ER solution and water were irradiated with an 808 nm laser with a power density of 1.5 W cm^{-2} for 400 s. Through a thermal imager (Fluke Ti32, Fluke Corporation, USA) and infrared imager, with increasing concentration, the heat generated by ICG-ER under laser irradiation also increased (**Figure 3A**). At a 160 μg/ml concentration, the temperature of laser irradiation for 240 s reached 65.2°C. These results indicate that ICG-ER can be used for photothermal therapy in tumors (**Figure 3B**).

In vivo photothermal therapy

ICG-ER has a good photothermal conversion rate and tumor targeting making ICG-ER feasi-

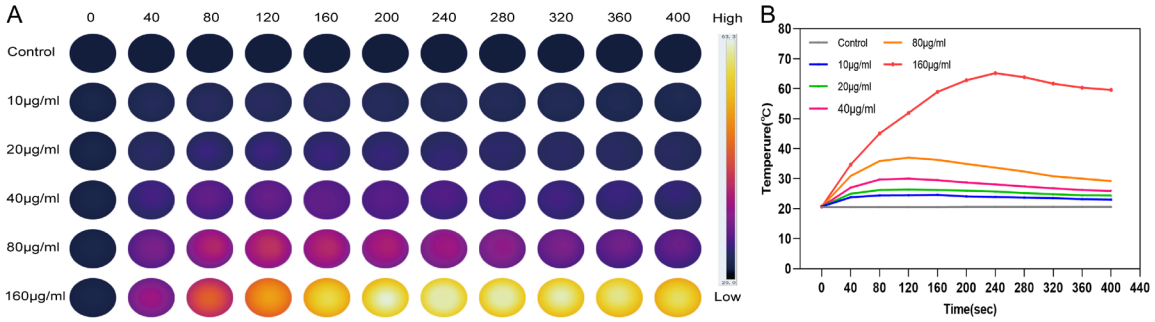

Figure 3. A. The corresponding IR thermal images of saline and ICG-ER different solution concentrations (10, 20, 40, 80, 160 μg/ml) at a stable power density of 808 nm laser (1.5 W/cm^{-2}). B. Temperature changes of ICG-ER and normal saline at different concentrations after laser irradiation for 400 s. The higher the concentration of ICG-ER, the higher the temperature. At a concentration of 160 μg/ml, ICG-ER produced a maximum of 65.2°C after laser irradiation.

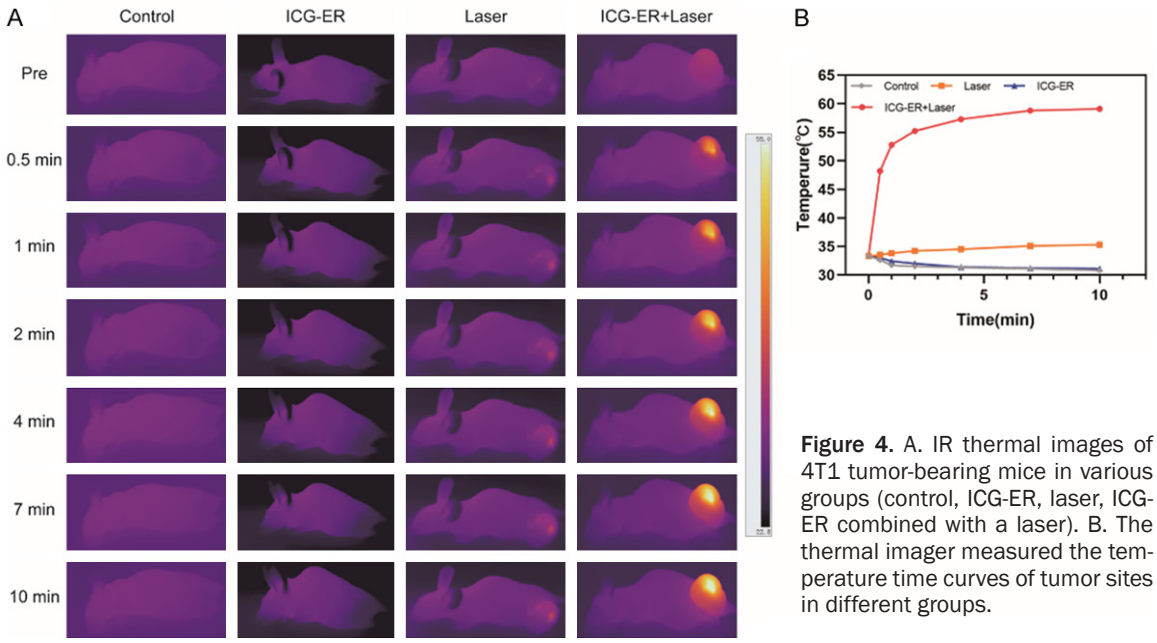

Figure 4. A. IR thermal images of 4T1 tumor-bearing mice in various groups (control, ICG-ER, laser, ICG-ER combined with a laser). B. The thermal imager measured the temperature time curves of tumor sites in different groups.

ble in photothermal therapy. To verify this, 4T1 tumor xenografts were established in nude mice. When the mice tumor volume reached 50-80 mm^3, ICG-ER was injected into the mice's tail vein, and normal saline was injected into the control group. According to the PA imaging results, after injection of ICG-ER and normal saline for 42 hours, 808 nm laser irradiation was carried out. The temperature change of the tumor site was recorded by an infrared thermal imaging camera (**Figure 4A**). The mice injected with ICG-ER were irradiated by an 808 nm laser (1.5 W cm^{-2}) and then heated rapidly (statistical temperature, **Figure 4B**).

The mice injected with normal saline and irradiated with the same laser had little temperature change. In contrast the mice injected with normal saline and ICG-ER but not irradiated with laser had no significant temperature change. The tumor volumes of mice treated with different methods were recorded (**Figure 5A**, **5B**). ICG-ER injection alone or laser irradiation had a little therapeutic effect on tumors in mice. Similarly, the tumors of mice injected with ICG-ER and irradiated with laser were eliminated without recurrence. During the 16-day observation period, there was no significant difference in the bodyweight of mice in each group (**Figure 5C**).

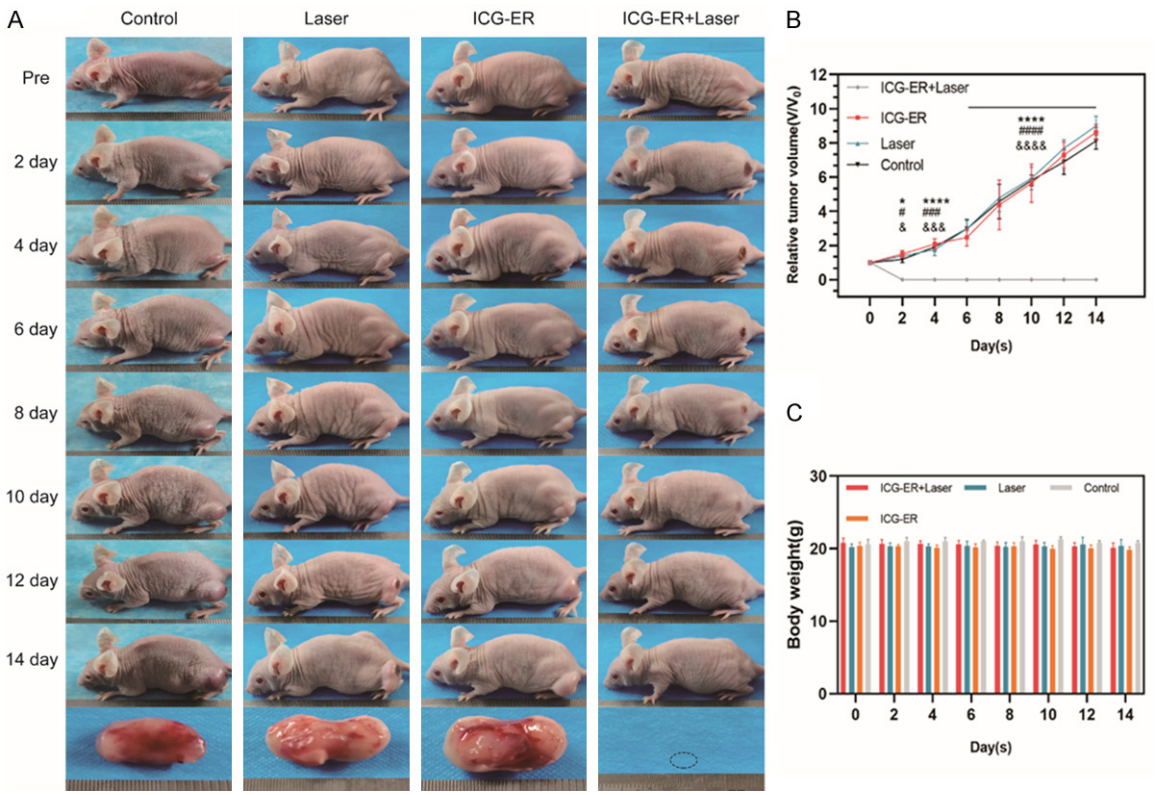

Figure 5. A. Photographs of changes in 4T1 tumor-bearing mice of different groups were recorded by cameras every two days during the 14 days. B. Relative tumor growth curves of the four groups after various treatments during the observation period. All data were tested for significance by two-way ANOVA. **P<0.01, ****P<0.0001 ICG-ER vs. ICG-ER+Laser, $^{\#}$P<0.05, $^{\#\#\#}$P<0.001, $^{\#\#\#\#}$P<0.0001 Laser vs. ICG-ER+Laser, $^{\&}$P<0.05, $^{\&\&\&}$P<0.001, $^{\&\&\&\&}$P<0.0001 Control vs. ICG-ER+Laser. (Values are means ± SD, n=3). C. The body weight curves of 4T1 tumor-bearing mice with various treatments for 14 days.

The histopathology results also verified the photothermal effect of ICG-ER. H&E staining showed that the tumor cells in the treatment group were necrotic. TUNEL and PCNA showed that apoptosis increased and proliferative cells decreased in the treatment group. HSP70 staining also showed that the expression of HSP70 in the treatment group was significantly increased (**Figure 6**). This indicates that ICG-ER has a good photothermal effect.

To test the biosafety of ICG-ER, one mouse in each group was taken for H&E staining of the main organs (heart, liver, spleen, lung, and kidney) (Figure S2). No apparent histopathological lesions were found. These results indicate that ICG-ER has high histocompatibility with the human body. At the same time, the blood of these mice was taken to detect liver and kidney function, and the results showed no significant change (Figure S3). This indicates that ICG-ER has high biological safety.

Discussion

Photoacoustic imaging can effectively show the structure and function of biological tissue with the help of a photosensitizer. It provides an important means to study biological tissue morphological structure, physiological characteristics, pathological characteristics, and metabolic function. Furthermore, it is especially suitable for early detection and treatment monitoring [30]. PTT uses PTCA with high-efficiency photothermal conversion. It is injected into the human body, uses targeted recognition technology to gather near tumor tissue, and converts light energy into heat energy under near-infrared light (NIR) irradiation to eliminate local tumors [31].

ICG is a tricarbocyanine dye with a near-infrared characteristic absorption peak approved by the US Food and Drug Administration (FDA) as a clinical near-infrared imaging reagent [32]. ICG

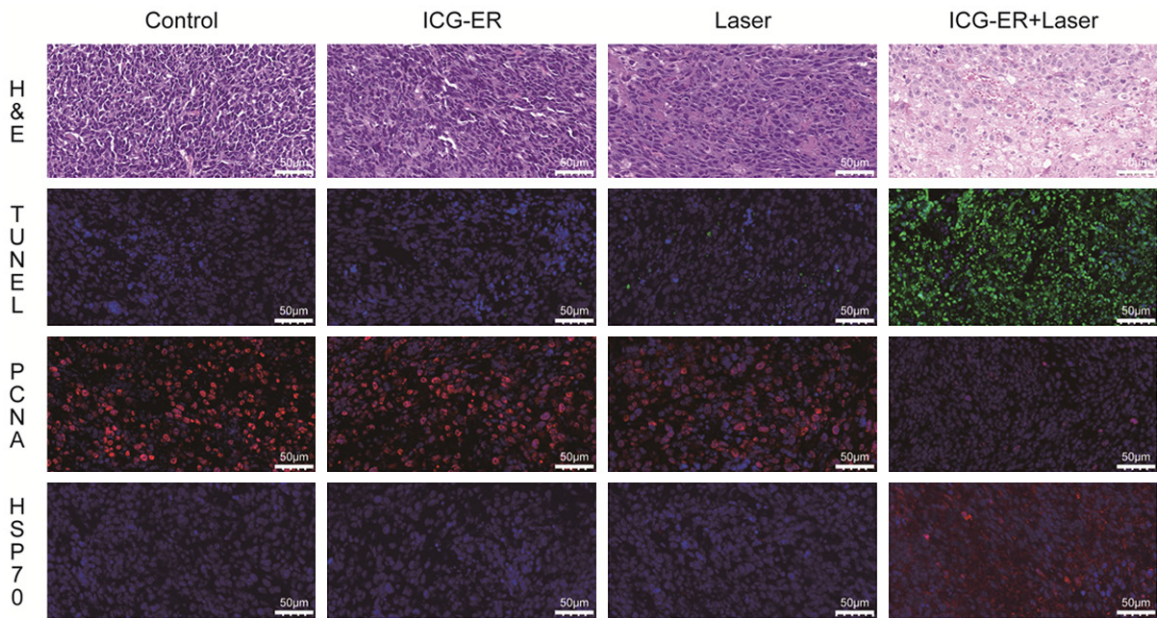

Figure 6. H&E, TUNEL, PCNA, and HSP70 staining of the tumor tissue at 1 day after various treatments. From top to bottom: H&E-stained cells, TUNEL-positive cells (green), PCNA-positive cells (red), and HSP70-positive cells (red). The DAPI-labeled nuclei are blue. The scale bars are 50 μm. All images were observed and retained by electron microscopy at 36.5X magnification.

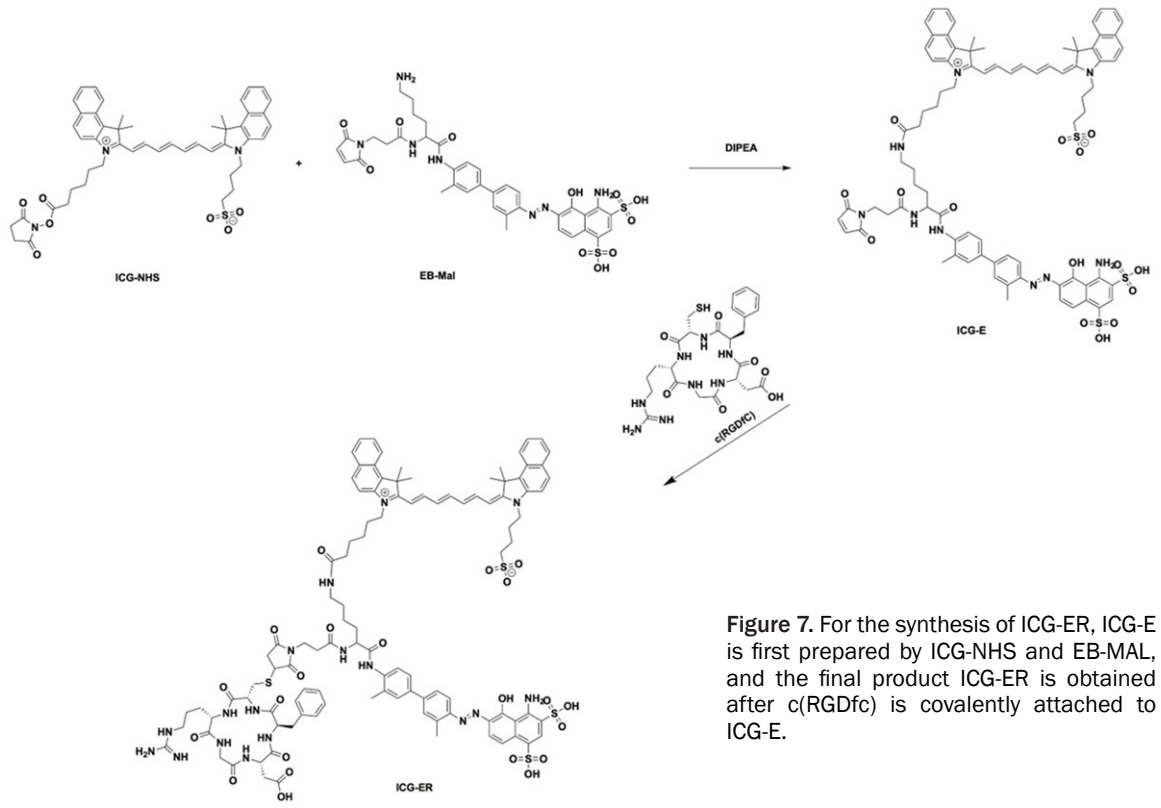

Figure 7. For the synthesis of ICG-ER, ICG-E is first prepared by ICG-NHS and EB-MAL, and the final product ICG-ER is obtained after c(RGDfc) is covalently attached to ICG-E.

can strongly absorb light energy and convert it into heat energy [33], making it suitable for use in photoacoustic imaging and photothermal therapy. In recent years, the research on the

treatment of ICG in breast cancer is in full swing, such as modifying ICG with hyaluronic acid and metal nanoparticles which can be degraded by tumor-specific hyaluronidase, so that ICG can be targeted by metal nanoparticles and can be degraded by tumor hyaluronidase into the interior of the tumor, so as to improve the efficacy of photothermal therapy of ICG in breast cancer [34]. However, in this study, the breast cancer tumors were not completely cleared, and the metal nanoparticles were made of rare metal, which made the preparation of the probe more expensive.

In addition to using metal nanoparticles to enhance the targeting of ICG, it is common to using RGD to directly modify ICG to enhance targeting. A study used internalized RGD (iRGD) to modify ICG liposomes to evaluate the efficacy of photothermal therapy and photodynamic therapy. The results show that iRGD-ICG-LPs has a good targeting for breast cancer, and the efficacy of photothermal therapy is significantly stronger than that of non-targeted ICG-LPs [35]. However, in order to give full play to the photothermal effect of ICG, we not only need to target ICG to the tumor tissue, but also need to increase the residence time of ICG in the tumor tissue, so as to achieve a better curative effect.

Some studies have shown that the use of albumin binder can prolong the blood circulation time of drug molecules [36, 37], which will prolong the time of imaging and therapy, so as to significantly increase the effective therapeutic dose and achieve better therapeutic results. As a widely used albumin binder, EB is an azo dye with a high affinity that can reversibly bind to human serum albumin *in vivo* and *in vitro* [20, 38]. When injected intravenously, EB can stably be combined with albumin in the blood. Due to its high water solubility and slow excretion, EB is widely used in biomedicine, such as evaluating blood volume and detecting lymph nodes and tumor location [39-41]. EB can be labeled with many molecular compounds. For example, derivatives such as NOTA-Evans Blue (NEB), have now been labeled with the nuclide ^{68}Ga and used clinically [42]. The uptake and retention time of nuclides in the tumor region was significantly prolonged after EB and radionuclide probe labeling [43], which led us to wonder whether EB combined with ICG could significantly improve the retention time and uptake degree of ICG in tumors. Related research has shown that the retention time of ICG-RGD in the tumor area is short, and the photoacoustic signal of the tumor tissue obviously declines at the 24th hour [44]. After using EB, the retention time of ICG-ER in tumor tissue was significantly longer than that of ICG-RGD alone, and the photoacoustic signal of tumor tissue remained at a high level from 12 h to 42 h, which significantly improved the timeliness of photothermal therapy of ICG.

We can draw the following conclusion from the above result: ICG-ER is a new albumin binding probe that can stably achieve targeted tumor imaging and photothermal therapy. ICG-ER shows the advantages of low toxicity and high targeting at both the cell and animal levels. *In vivo* photoacoustics showed perfect binding and retention times at the tumor site, which makes ICG-ER a good potential in PA. ICG is a good PTCA. After the modification of EB and RGD, the stability of ICG-ER *in vivo* is enhanced, and it has an excellent photothermal conversion rate. Related studies have proved that the growth of tumor cells will be inhibited when the temperature of tumor site reaches 47°C or higher [45]. In the study of photothermal effects *in vitro*, ICG-ER increased rapidly and obviously after laser irradiation, and the temperature reached 65°C at the concentration of 160 μg/ml. This advantage gives ICG-ER a guiding significance in applying targeted photothermal therapy, and after 16 days of photothermal therapy, there is no recurrence in the tumor site. In general, ICG-ER has potential in the optical imaging and photothermal treatment of malignant tumors.

Acknowledgements

The authors gratefully acknowledge the financial support from the National Natural Science Foundation of China (NSFC) [Grant Nos. 82102093] and the Natural Science Foundation of Chongqing [cstc2021jcyj-msxmX0006].

Disclosure of conflict of interest

None.

Address correspondence to: Dr. Peng-Fei Xu, Institute of Clinical Pharmacy & Pharmacology,

Jining First People's Hospital, Jining Medical University, Jining 272000, P. R. China. E-mail: pengfeixucsu@outlook.com; Hua Pang, Department of Nuclear Medicine, The First Affiliated Hospital of Chongqing Medical University, No. 1 Youyi Road, Chongqing 400016, P. R. China. E-mail: phua1973@163.com

References

[1] Gefferth K. Diagnostic and therapeutic considerations of X-Ray hazard and protection in infants and children. 1962.

[2] Chang RF, Wu WJ, Moon WK and Chen DR. Automatic ultrasound segmentation and morphology based diagnosis of solid breast tumors. Breast Cancer Res Treat 2005; 89: 179-185.

[3] Lee CH. Problem solving MR imaging of the breast. Radiol Clin North Am 2004; 42: 919-34.

[4] Valluru KS, Wilson KE and Willmann JK. Photoacoustic imaging in oncology: translational preclinical and early clinical experience. Radiology 2016; 280: 332-349.

[5] Harbeck N and Gnant M. Breast cancer. Lancet 2017; 389: 1134-1150.

[6] Turner NC, Neven P, Loibl S and Andre F. Advances in the treatment of advanced oestrogen-receptor-positive breast cancer. Lancet 2017; 389: 2403-2414.

[7] Early Breast Cancer Trialists' Collaborative Group (EBCTCG), Peto R, Davies C, Godwin J, Gray R, Pan HC, Clarke M, Cutter D, Darby S, McGale P, Taylor C, Wang YC, Bergh J, Di Leo A, Albain K, Swain S, Piccart M and Pritchard K. Comparisons between different polychemotherapy regimens for early breast cancer: meta-analyses of long-term outcome among 100,000 women in 123 randomised trials. Lancet 2012; 379: 432-44.

[8] Cheng L, Wang C, Feng L, Kai Y and Zhuang L. Functional nanomaterials for phototherapies of cancer. Chin Clin Oncol 2014; 114: 10869-10939.

[9] Gnanasammandhan MK, Idris NM, Bansal A, Kai H and Yong Z. Near-IR photoactivation using mesoporous silica-coated NaYF4: Yb,Er/Tm upconversion nanoparticles. Nat Protoc 2016; 11: 688-713.

[10] Karimi M, Sahandi Zangabad P, Baghaee-Ravari S, Ghazadeh M, Mirshekari H and Hamblin MR. Smart nanostructures for cargo delivery: uncaging and activating by light. J Am Chem Soc 2017; 139: 4584-4610.

[11] Chu KF and Dupuy DE. Thermal ablation of tumours: biological mechanisms and advances in therapy. Nat Rev Cancer 2014; 14: 199-208.

[12] Chen R, Wang J and Qiao H. Organic photothermal conversion materials and their application in photothermal therapy. Progress in Chemistry 2017.

[13] Mielke D, Malinova V and Rohde V. Comparative analysis of endoscopic versus microscopic ICG-angiography in aneurysm surgery. Surg Endosc 2011; 25: 3957-3958.

[14] Tomoharu S, Abdelazeem KK, Megumi T, Takashi H, Kazuhiko Y, Yoshikazu M and Masakazu T. A novel method for sentinel lymph node biopsy by indocyanine green fluorescence technique in breast cancer. Cancers 2010; 2: 713-720.

[15] Murawa D, Hirche C, Dresel S and Hünerbein M. Sentinel lymph node biopsy in breast cancer guided by indocyanine green fluorescence. Br J Surg 2009; 96: 1289-1294.

[16] Hirche C, Murawa D, Mohr Z, Kneif S and Hünerbein M. ICG fluorescence-guided sentinel node biopsy for axillary nodal staging in breast cancer. Breast Cancer Res Treat 2010; 121: 373-378.

[17] Shimizu S, Kamiike W, Hatanaka N, Yoshida Y and Matsuda H. New method for measuring ICG Rmax with a clearance meter. World J Surg 1995; 19: 113-118.

[18] Hagen A, Grosenick D, Macdonald R, Rinneberg H and Schlag PM. Late-fluorescence mammography assesses tumor capillary permeability and differentiates malignant from benign lesions. Opt Express 2009; 17: 17016-17033.

[19] Poellinger A, Burock S, Grosenick D, Hagen A, Lüdemann L, Diekmann F, Engelken F, Macdonald R, Rinneberg H and Schlag PM. Breast cancer: early- and late-fluorescence near-infrared imaging with indocyanine green--a preliminary study. Radiology 2011; 258: 409-16.

[20] Evans HM and Schulemann W. The action of vital stains belonging to the benzidine group. Science 1914; 39: 443-454.

[21] Bobin JY, Zinzindohoue C, Isaac S, Saadat M and Roy P. Original paper tagging sentinel lymph nodes: a study of 100 patients with breast cancer. Eur J Cancer 1999; 35: 569-73.

[22] Xiong JP, Stehle T, Zhang R, Joachimiak A, Frech M, Goodman SL and Arnaout MA. Crystal structure of the extracellular segment of integrin αVβ3 in complex with an Arg-Gly-Asp ligand. Science 2002; 296: 151-155.

[23] Yun W, Cai W and Chen X. Near-infrared fluorescence imaging of tumor integrin αvβ3 expression with Cy7-labeled RGD multimers. Mol Imaging Biol 2006; 8: 226.

[24] Chen X, Park R, Hou Y, Khankaldyyan V, Gonzales-Gomez I, Tohme M, Bading JR, Laug WE and Conti PS. MicroPET imaging of brain tumor angiogenesis with 18F-labeled PEGylated RGD

peptide. Eur J Nucl Med Mol Imaging 2004; 31: 1081-1089.
[25] Tsiapa I, Loudos G, Varvarigou A, Fragogeorgi E, Psimadas D, Tsotakos T, Xanthopoulos S, Mihailidis D, Bouziotis P and Nikiforidis GC. Biological evaluation of an ornithine-modified 99mTc-labeled RGD peptide as an angiogenesis imaging agent. Nucl Med Biol 2013; 40: 262-272.
[26] Gellerman G. Novel targeted non-RGD cyclic peptide drug conjugates for treatment of human metastatic melanoma. Oncotarget 2017; 8: 757-768.
[27] Wang XS, Huang Y, Liu D, Liang L and Liu JP. RGD modified docetaxel and suramin loaded liposome for breast cancer targeting therapy. Chinese Journal of Cancer Prevention and Treatment 2014; 21: 1783-1793.
[28] Xu P, Hu L, Yu C, Yang W, Kang F, Zhang M, Jiang P and Wang J. Unsymmetrical cyanine dye via in vivo hitchhiking endogenous albumin affords high-performance NIR-II/photoacoustic imaging and photothermal therapy. J Nanobiotechnology 2021; 19: 334.
[29] Lee N, Choi SH and Hyeon T. Nano-sized CT contrast agents. Adv Mater 2013; 25: 2641-2660.
[30] Liu Y, Teng L, Liu HW, Xu C and Tan W. Recent advances in organic-dye-based photoacoustic probes for biosensing and bioimaging. Science China Chemistry 2019.
[31] Shanmugam V, Selvakumar S and Yeh CS. Near-infrared light-responsive nanomaterials in cancer therapeutics. Chem Soc Rev 2014; 43: 6254-87.
[32] Moody ED, Viskari PJ and Colyer CL. Non-covalent labeling of human serum albumin with indocyanine green: a study by capillary electrophoresis with diode laser-induced fluorescence detection. J Chromatogr B Biomed Sci Appl 1999; 729: 55-64.
[33] Yaseen MA. Photothermal and photochemical effects of laser light absorption by indocyanine green (ICG). Proc Spie 2005; 5695: 27-35.
[34] Liu R, Hu C, Yang Y, Zhang J and Gao H. Theranostic nanoparticles with tumor-specific enzyme-triggered size reduction and drug release to perform photothermal therapy for breast cancer treatment. Acta Pharm Sin B 2019; 9: 410-420.
[35] Yan F, Wu H, Liu H, Deng Z, Liu H, Duan W, Liu X and Zheng H. Molecular imaging-guided photothermal/photodynamic therapy against tumor by iRGD-modified indocyanine green nanoparticles. J Control Release 2016; 224: 217-228.
[36] Heneweer C, Holland JP, Divilov V, Carlin S and Lewis JS. Magnitude of enhanced permeability and retention effect in tumors with different phenotypes: 89Zr-albumin as a model system. J Nucl Med 2011; 52: 625-633.
[37] Dumelin CE, Trüssel S, Buller F, Trachsel E, Bootz F, Zhang Y, Mannocci L, Beck SC, Drumeamirancea M and Seeliger MW. A portable albumin binder from a DNA-encoded chemical library. Angew Chem Int Ed Engl 2010; 47: 3196-3201.
[38] Oskar S and Igor K. Selective vulnerability of the blood-brain barrier in chemically induced lesions. J Neuropathol Exp Neurol 1966; 25: 542-59.
[39] Roller BT, Munson JM, Brahma B, Santangelo PJ, Pai SB and Bellamkonda RV. Evans blue nanocarriers visually demarcate margins of invasive gliomas. Drug Deliv Transl Res 2015; 5: 116-24.
[40] Radu M and Chernoff J. An in vivo assay to test blood vessel permeability. J Vis Exp 2013; e50062.
[41] Tsopelas C, Bevington E, Kollias J, Shibli S, Farshid G, Coventry B and Chatterton BE. 99mTc-Evans blue dye for mapping contiguous lymph node sequences and discriminating the sentinel lymph node in an ovine model. Ann Surg Oncol 2006; 13: 692-700.
[42] Zhang J, Lang L, Li F, Zhu Z, Niu G and Chen X. Clinical translation of an albumin-binding PET radiotracer 68Ga-NEB. J Nucl Med 2015; 1609-1614.
[43] Rui T, Orit J, Gang N, Kiesewetter DO, Wang Z, Zhu G, Ma Y, Gang L and Chen X. Evans blue attachment enhances somatostatin receptor subtype-2 imaging and radiotherapy. Theranostics 2018; 8: 735-745.
[44] Martina C, Francesco B, Giovanni V, Paolo O, Claudia C, Federica B, Alessia C, Lorena P, Alessandro M and Luisa P. Photoacoustic imaging of integrin-overexpressing tumors using a novel ICG-based contrast agent in mice. Photoacoustics 2018; 11: 36-45.
[45] Ghaffari H, Beik J, Talebi A, Mahdavi SR and Abdollahi H. New physical approaches to treat cancer stem cells: a review. Clin Transl Oncol 2018; 20: 1-20.

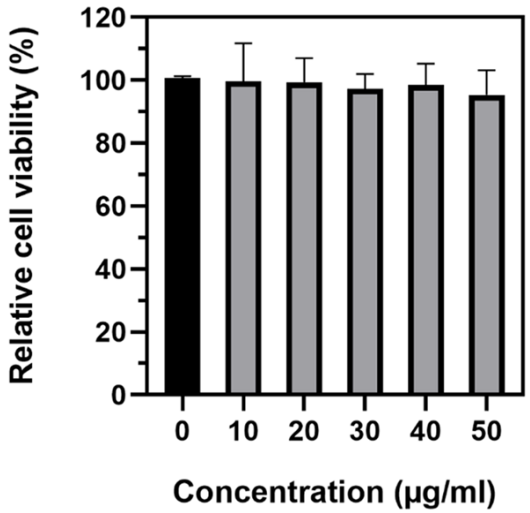

Figure S1. Cell viability of 4T1 cells after incubation with EB-ICG-RGD at different concentrations for 24 h.

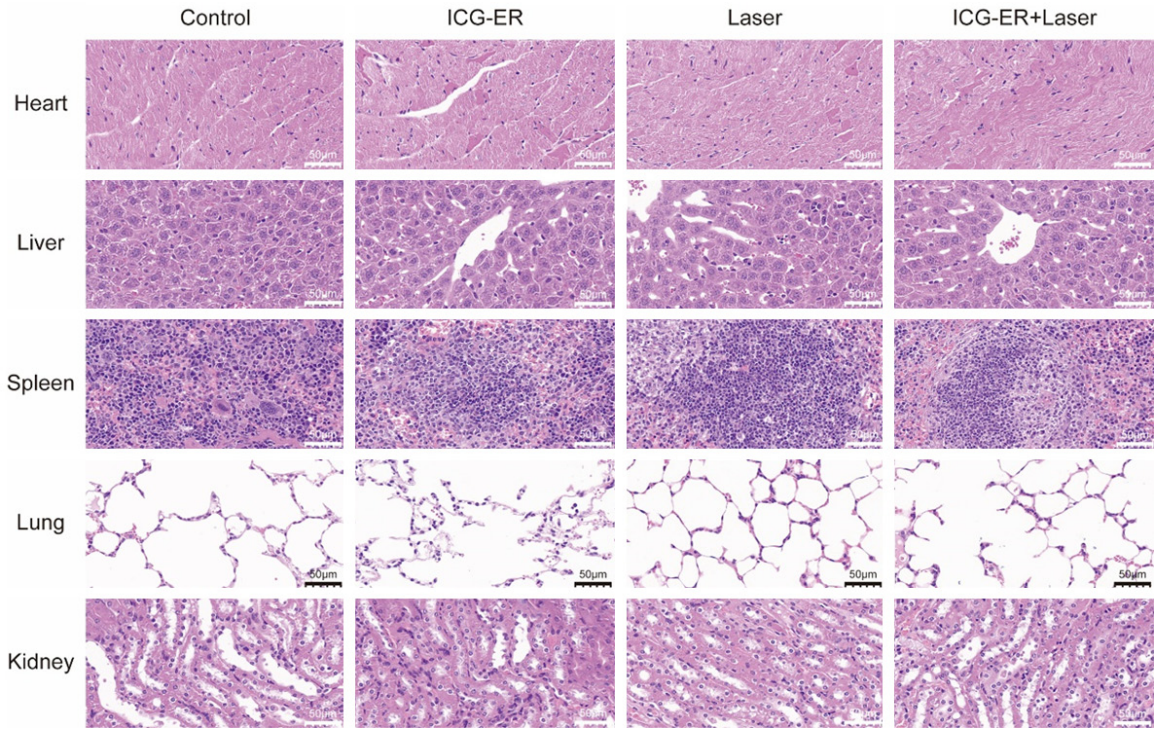

Figure S2. H&E staining of the major organs (heart, liver, spleen, lung, and kidney) of 4T1 tumor-bearing mice after different treatments. The scale bars are 50 μm. All images were observed and retained by electron microscopy at 36.5X magnification.

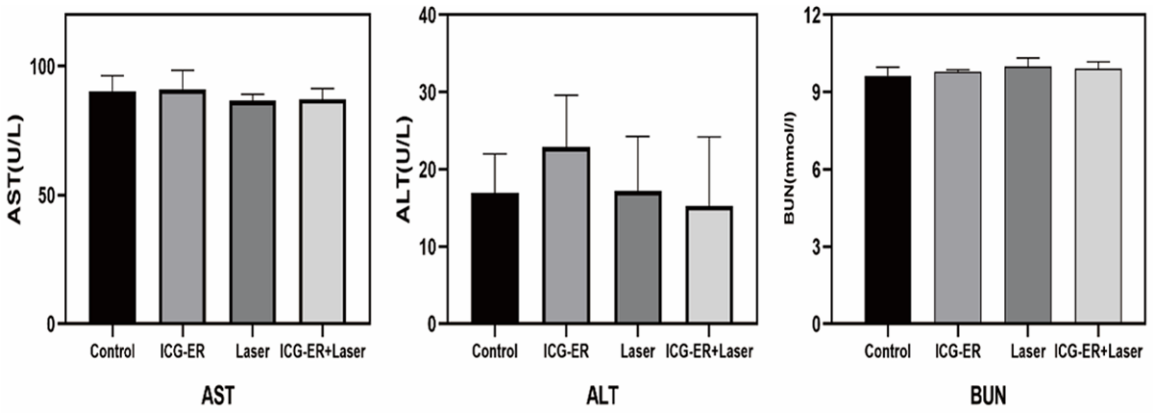

Figure S3. ALT, AST and BUN of the tumor tissue at 1 day after various treatments. All the indicators are within the normal range.

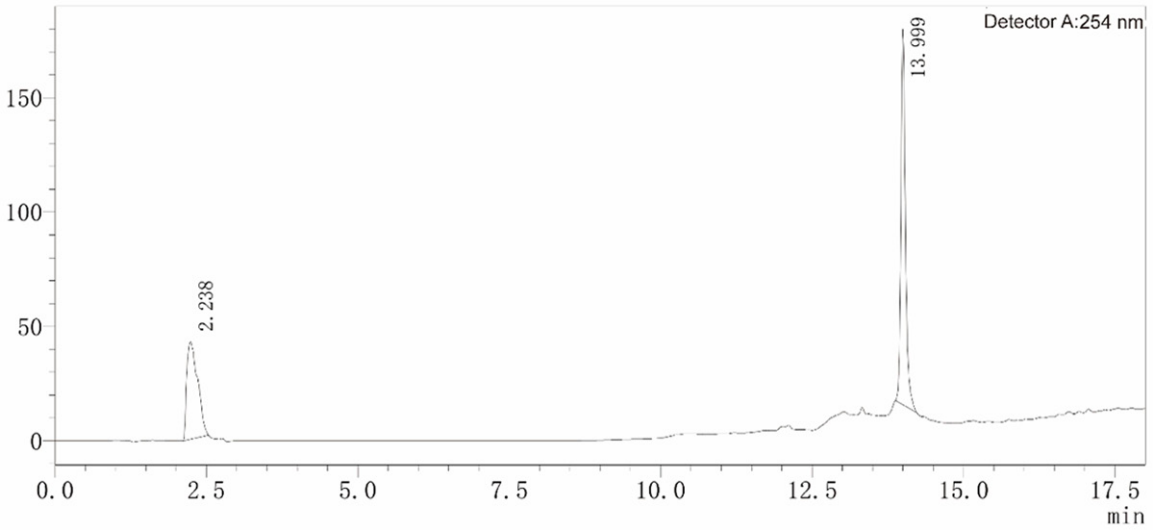

Figure S4. HPLC chromatogram (254 nm) of ICG-E.

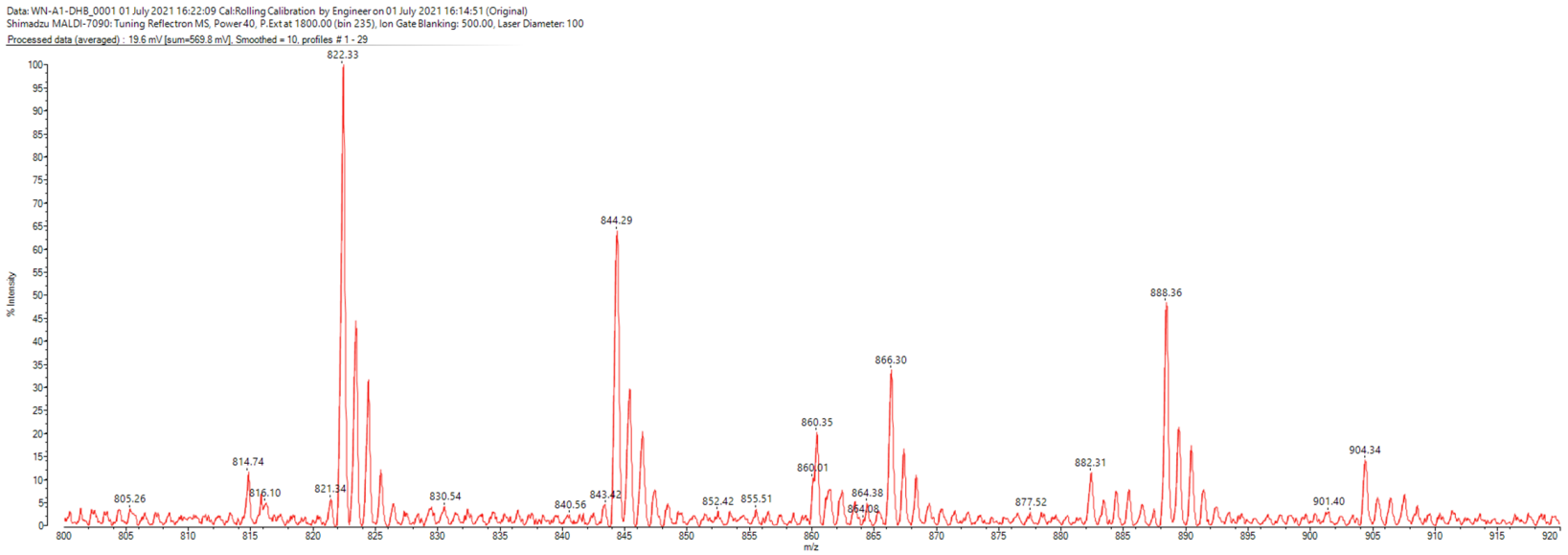

Figure S5. MALDI-TOF-MS measurement of EB-Mal.

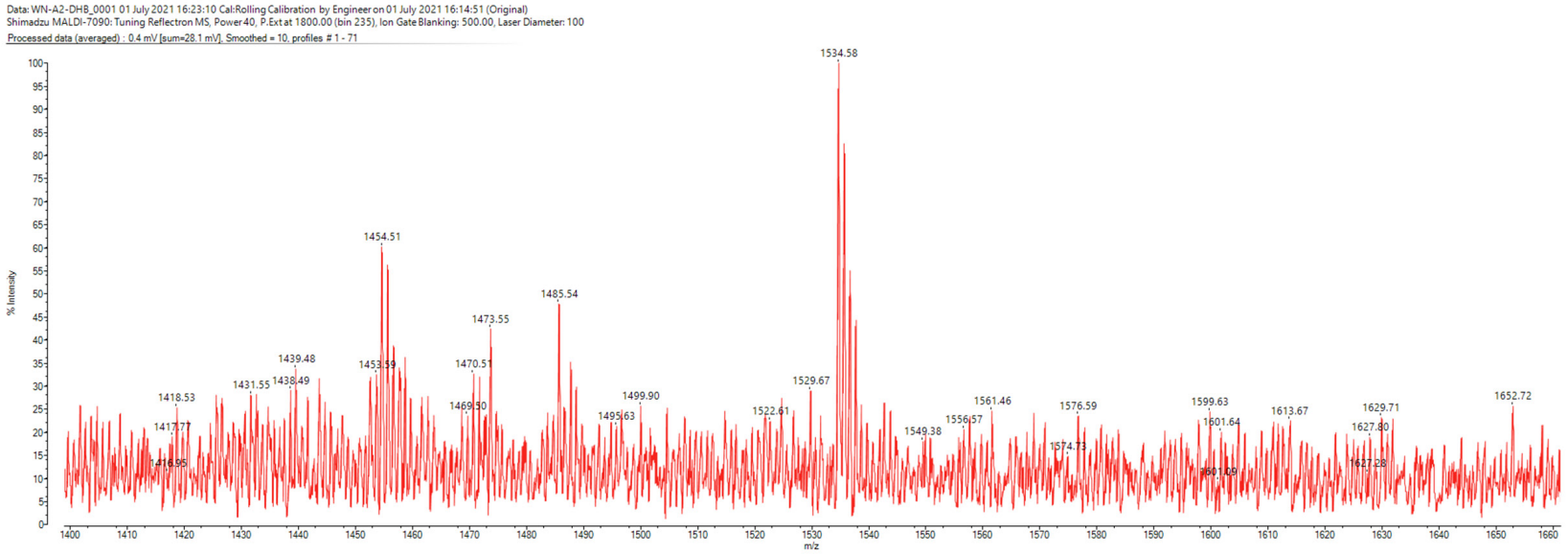

Figure S6. MALDI-TOF-MS measurement of ICG-E.

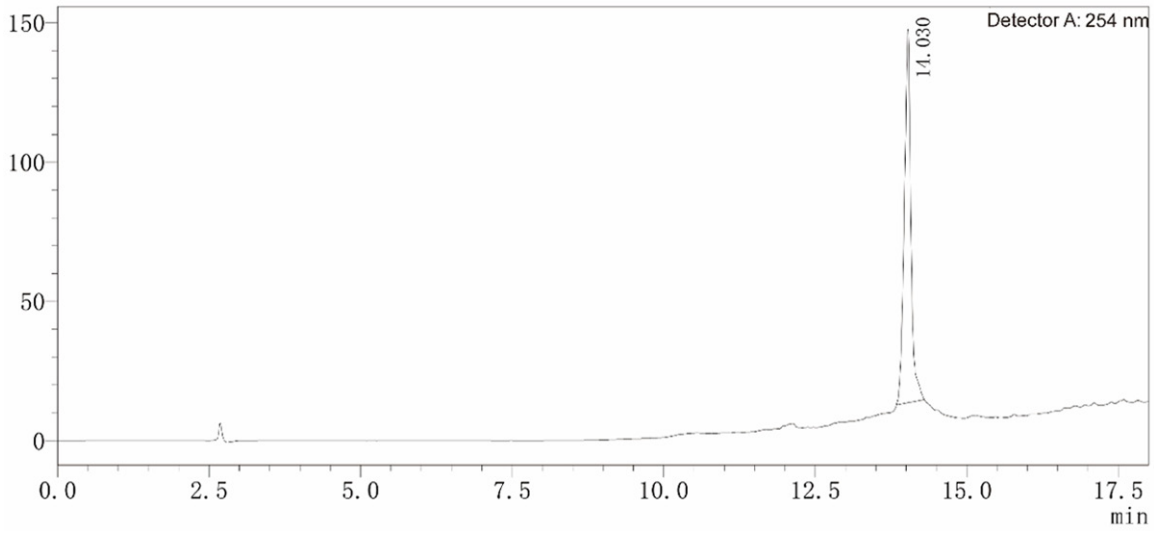

Figure S7. HPLC chromatogram (254 nm) of ICG-ER.

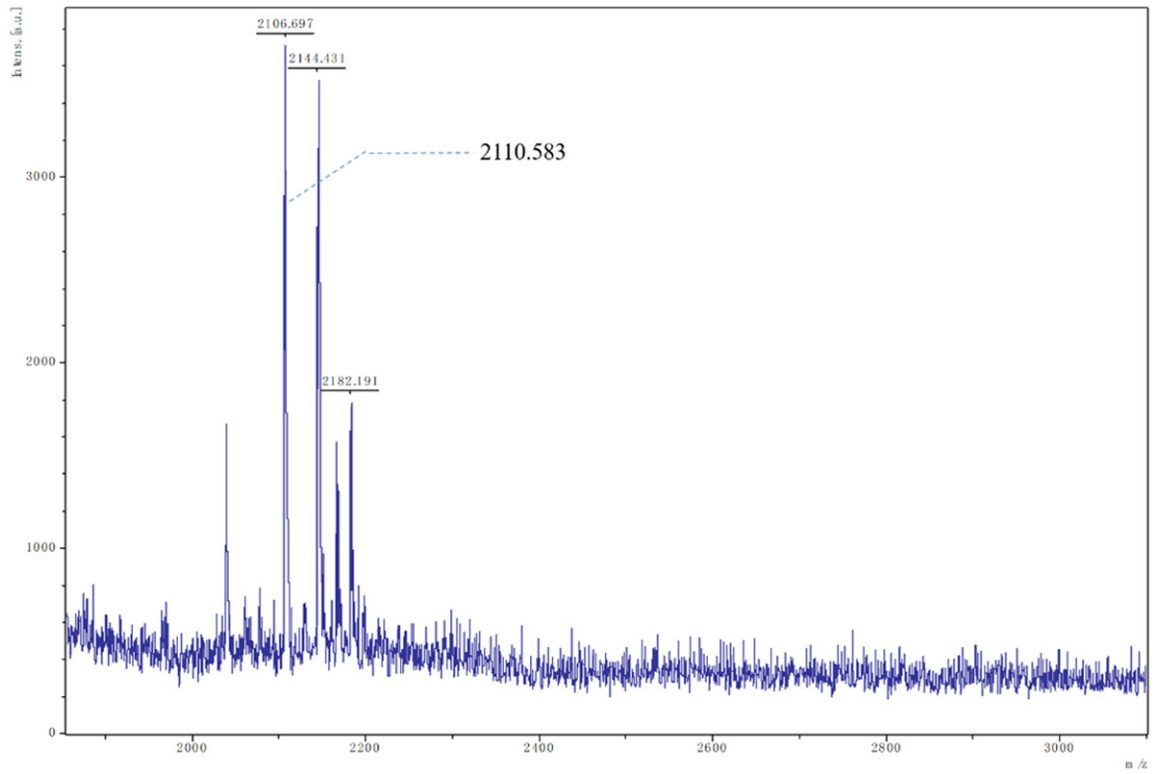

Figure S8. MALDI-TOF-MS measurement of ICG-ER.

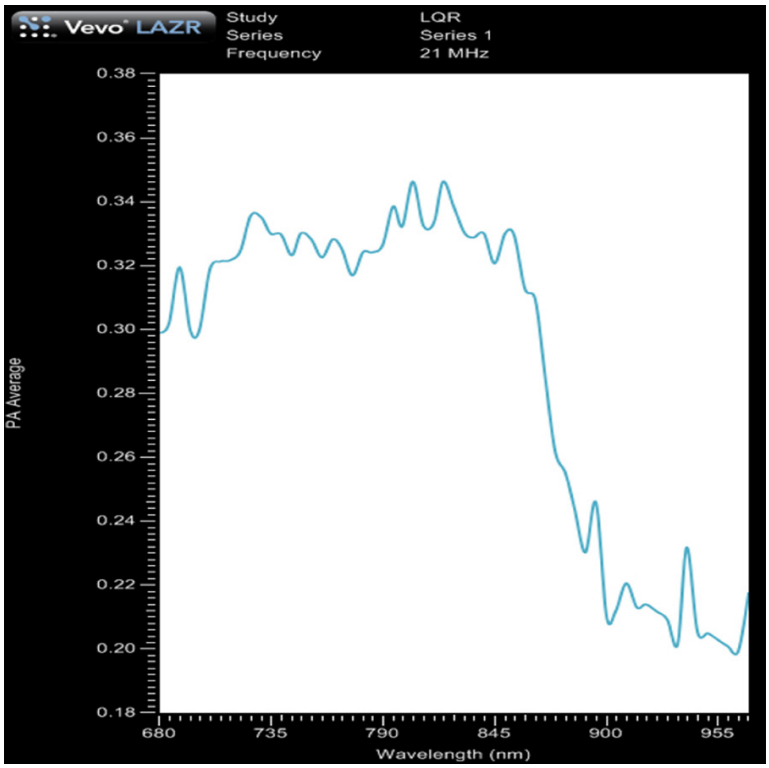

Figure S9. The most optimal wavelength for PA imaging by full-wavelength scanning.